Structure and Mechanical Response of Self-Assembled Poly(butadiene)-*b*-poly(ethylene oxide) Colloids Probed by Atomic Force Microscopy

Shuliang Li and Andre F. Palmer*

Department of Chemical and Biomolecular Engineering, University of Notre Dame, Notre Dame, Indiana 46556

Received October 15, 2004; Revised Manuscript Received April 12, 2005

ABSTRACT: In this study, the aqueous structure and mechanical response of self-assembled poly(butadiene)-*b*-poly(ethylene oxide) (PB−PEO) colloids were probed using atomic force microscopy (AFM). It was observed that the structure of these colloids ranged from spherical micelles, wormlike micelles, to polymersomes depending on the diblock composition and method of preparation. At 1 mg/mL of PB−PEO, ordered micelles exhibiting hexagonal packing was observed on glass surfaces. Isotropic wormlike micelles with network and spaghetti-like patterns were also observed. AFM force imaging of closely packed micelles on glass surfaces showed a sharp downward deflection, which implied the existence of a "transition escape" most probably due to a conformational change in the PEO hydrophilic brush upon AFM tip compression. Force curve measurements on micelles and polymersomes indicated that the hydrophobic core has a springlike linear response, while the hydrophilic PEO corona has an exponential response to the applied AFM tip compression force. Taken together, the results of this study shed new light on the structure and mechanical response of self-assembled PB−PEO colloids as a function of copolymer composition and method of preparation.

1. Introduction

Research on liposomes as potential drug delivery vehicles has been ongoing for several decades.[1−3] Recent studies demonstrated that block copolymer micelles could be used to enhance loading and retention of hydrophobic drugs.[4−8] Similar to natural phospholipids, amphiphilic block copolymers composed of a hydrophobic domain and a hydrophilic domain are thermodynamically driven to self-assemble into various ordered structures such as spherical micelles, wormlike micelles, and closed bilayer structures (polymersomes) depending on the volume/mass fraction of the hydrophilic to hydrophobic blocks.[7−9] Unlike liposomes, block copolymer vesicles are far more robust under strain and less permeable to water.[7,10] Because of the larger molecular weight of block copolymers, usually >1 kDa, the hydrophobic cores of these vesicles are thicker compared to liposomes composed of natural lipids. A direct consequence of possessing a larger hydrophobic core confers onto polymer vesicles the ability to encapsulate larger amounts of hydrophobic or amphiphilic drugs per unit mass of block copolymer.[11]

Amphiphilic diblocks have been synthesized with hydrophilic blocks composed of poly(ethylene glycol) (PEG) that confers more resistance to plasma protein deposition and extends vesicle circulation lifetime in vivo. [12] The use of PEG blocks makes it possible to form self-assembled structures that are 100% PEGylated, compared to liposomes which can only be PEGylated up to 11% (mole fraction of the lipid membrane that is PEGylated).[13,14] Given the current use of self-assembled PEGylated diblock colloids in various drug delivery applications, it is important to characterize their structural properties in aqueous solution in order to mimic their structure in vivo.

The structure of block copolymer micelles on different solid substrates (mica, glass, and carbon) was probed in the dried state using atomic force microscopy (AFM).[15−17] Samples were typically prepared by coating diblock films (dissolved in organic solvent) onto substrates and subsequently evaporating the solvent to trap the micellar structures. Interestingly, Regenbrecht et al.[18] applied AFM in tapping mode to image predried poly(ethylethylene)-*b*-poly(styrenesulfonic acid) (PEE−PSSH) polymer micelles in air and observed that PEE−PSSH micelles switched their morphology from spherical micelles to network-like structures upon varying the ionic strength.

Surprisingly, few AFM studies have investigated the structure of "wet" absorbed block copolymer micelles. In a study focusing on the effect of pH on the self-assembled structure of poly(2-(dimethylamino)ethyl methacrylate)-*b*-poly(methyl methacrylate) (PDMA-*b*-PMMA) colloids, Webber et al.[19] observed micelles and hexagonal close-packed micellar structures on mica using AFM in situ. In recent work, Hamley and coworkers[20,21] investigated the micellar structure of poly(ethylene oxide)-*b*-poly(propylene oxide) block copolymers on both hydrophobic silica and hydrophilic mica as a function of micelle concentration. Force curves on these micelles were also obtained which provided insight into the mechanical properties of block copolymer micelles, especially the brushlike hydrophilic dense layers, which could not be distinguished from AFM topology imaging.

In this study, we investigated the self-assembled structure and mechanical response of a series of poly(butadiene)-*b*-poly(ethylene oxide) (PB−PEO) diblocks with different hydrophilic fractions via AFM topology and force imaging prepared by various protocols. Since these self-assembled colloids are currently being investigated as potential drug delivery vehicles, we wanted to examine the structure of these colloids under relatively physiological conditions. In fact, different morphologies of block copolymer colloids are expected to possess different drug loading capacities and release

10.1021/ma047858j CCC: $30.25
Published on Web 05/25/2005

Table 1. Molecular Characteristics of PB−PEO Diblocks and Self-Assembled Colloid Structure in PBS[a]

diblock	M_n (kg/mol)	N_{PB}	N_{PEO}	w_{PEO}	PDI	bulk rehydration	film rehydration
$PB_{96}-PEO_{52}$	7.3	96	52	0.32	1.06	N	N, C, Cy
$PB_{219}-PEO_{121}$	17.1	219	121	0.31	1.04	B	B
$PB_{407}-PEO_{286}$	34.6	407	286	0.36	1.06	S	B + S

[a] M_n = number-average molecular weight, N_{PB} = number of monomer repeat units in PB block, N_{PEO} = number of monomer repeat units in PEO block, w_{PEO} = weight fraction of PEO block in diblock copolymer, and PDI = polydispersity index. Morphologies determined by AFM: B = bilayers; C = cylindrical worms, S = spherical micelles, Cy = cylindrical worms with Y-junctions, N = networks.

kinetics.[22] Although AFM can only probe the topography of adsorbed species on a substrate surface, it is the best technique available to produce high-resolution 3-D topographic images in aqueous and physiologically relevant environments without the need to stain the specimen.[23]

In previous work, the structure of PB−PEO colloids was extensively studied as a function of copolymer molecular weight, degree of polymerization, hydrophilic block weight fraction, and composition of binary blends of diblocks using cryogenic transmission electron microscopy (cryo-TEM).[24,25] Morphology diagrams correlating PB−PEO aggregate structure in water were constructed as a function of the molecular composition. It was demonstrated that as the hydrophilic content (w_{PEO}) was increased, a sequence of structures was observed beginning with closed bilayers (in the form of vesicles, also known as polymersomes), then wormlike micelles, and then spherical micelles separated by composition windows containing mixed morphologies.

To the best of our knowledge, no work has been done to study various structures of PB−PEO colloids in aqueous solution using AFM, although Dalhaimer et al.[26] recently reported AFM imaging of wormlike micelles composed of hydrogenated PB in PEO−PEE. In our work, three typical morphologies, namely, spherical micelles, polymersomes, and wormlike micelles (with network patterns), were observed via AFM imaging in aqueous solution. AFM force curves were also obtained on these different self-assembled diblock structures to provide further insight into the mechanical response of both the hydrophilic brush layer and the hydrophobic core of these colloids. We observed two distinct "escape transitions" for force curves obtained on micelles in contact mode, which verified a theoretical prediction made by Sevick and co-workers that block polymer chains confined under a finite-sized obstacle undergo multiple escape transitions above a critical compression.[27,28]

2. Experimental Section

2.1. Materials. PB−PEO block copolymers with various molecular weights and degrees of polymerization (Table 1) were purchased from Polymer Source (Montreal, QC, Canada). Polycarbonate membranes were purchased from Avanti Polar Lipids, Inc. (Birmingham, AL). All water was taken from a Barnstead E-Pure (Barnstead/Thermolyne, Dubuque, IA) ultrapure deionization water system with a resistivity of 18.1 MΩ cm and filtered through 0.02 μm inorganic membrane filters obtained from Whatman (Maidstone, England). Phosphate buffered saline (PBS) at physiological pH 7.3 was made using phosphate salts and NaCl obtained from Sigma-Aldrich (St. Louis, MO).

2.2. Diblock Copolymer Self-Assembled Colloid Preparation. Diblock copolymer self-assembled colloids were prepared by either bulk rehydration or film rehydration as reported by Discher et al.[29] For bulk rehydration, diblock colloids were prepared by placing 10 mg of diblock copolymers in 1 mL of filtered PBS buffer with overnight stirring. For film rehydration, 1 mL of 10 mg/mL of polymer dissolved in chloroform was dried in a round-bottom flask by rotary evaporation of the solvents at 37 °C to ensure complete removal of chloroform.[30−32] Addition of 1 mL of PBS buffer to the resultant dried copolymer film led to spontaneous budding of vesicles off the round-bottom glass surface into solution. Rehydrated copolymer solutions were then sonicated for 3 min and subsequently extruded with 25 passes through 400 nm pore diameter polycarbonate membranes obtained from Avanti Polar Lipids (Alabaster, AL).[33] Resultant diblock copolymer colloids were diluted 10 times in preparation for AFM imaging.

2.3. Atomic Force Microscopy. All imaging was performed using a Digital Instruments (Santa Barbara, CA) Nanoscope IV Multimode AFM system equipped with a vertical E scanner (15 × 15 μm scan size and 3.64 μm vertical range) in fluid Tapping Mode. Cantilevers with 100 μm, narrowed-leg, oxide-sharpened Si_3N_4 tips with a nominal spring constant of ∼0.22 N/m were mounted in the AFM tapping-mode fluid cell. The overall resonance frequency of the fluid cell and the probe assembly was 8 ± 1 kHz. The tapping force, calculated as the ratio of engaged to free amplitude cantilever oscillation (A_{sp}/A_0), was maintained at 0.8−0.9 (soft tapping)[34] to minimize sample deformation.

Muscovite mica disks obtained from SPI Supplies (West Chester, PA) were used freshly cleaved. Microscope cover glass slides obtained from Fisher Scientific (Pittsburgh, PA) were first cleaned and stored in 20 vol % HCl in ethanol. Glass slides were then washed repeatedly with deionized water and dried with a contaminant-free commercial air duster. To assess the relative roughness of these two surfaces, the root-mean-square (rms) roughness (δ) of freshly cleaved mica and clean cover glass slides was measured to be 0.047 and 0.179 nm, respectively, by probing the various substrate surfaces in PBS buffer via AFM in contact mode. Substrates (mica or glass) were affixed to AFM specimen disks obtained from Ted Pella, Inc. (Redding, CA) using commercial epoxy. Before imaging, the tapping mode fluid cell and silicone S-profile O-ring (Veeco Metrology, Santa Barbara, CA) were sonicated in soap water for 1 h and washed repeatedly with deionized water and then dried with contaminant-free commercial air duster. Block copolymer assemblies dispersed in aqueous solution were first incubated on mica or glass for 1 h to promote sample absorption onto the substrate surface. After the fluid cell and slide were mounted onto the AFM, PBS buffer was pumped through silicone rubber tubing into the fluid cell sealed by the S-profile O-ring. Height- and amplitude-mode images were collected at 512 × 512 pixel resolution at a scanning rate of 0.5 Hz and a scan angle of 0°. Processing and analysis of images were carried out using the off-line analysis program provided by Digital Instruments software version 5.12r3 (Veeco Metrology Group, Santa Barbara, CA). Height images were flattened and first-order plane fitted before performing off-line zoom, section, and surface analyses.

All force curves were obtained in contact mode except for data shown in Figure 9E. After a good image of diblock colloids was obtained in Tapping Mode, the AFM was switched to contact mode to measure the force curve. The calibrated spring constant (0.22 N/m) which was obtained using the deflection method against a reference cantilever (Park Scientific Instruments, CA) of known spring constant (0.157 N/m) was used in all force curve calculations. Force curves were obtained on bare mica and glass surfaces rinsed with PBS buffer and on all diblock copolymer colloids. Force curves were also probed around diblock colloids to ensure that the force curves repre-

sented the interaction between the tip and the diblock colloids and not the tip and the substrate surface. The typical time for a complete force curve cycle (extension and retraction) was ~1 s. Force curves were collected at 2048 × 2048 data points and converted to force−displacement curves by defining the point of highest loading and the point of zero force as described in the literature.[35,36] The dimensions of PB−PEO colloids measured using AFM are apparent values obtained from section analyses without correction, except for the diameter of PB_{96}−PEO_{52} wormlike micelles in water (Figure 5) which is corrected for the broadening effect due to the finite radius of the AFM as described by LaRue et al.[37]

2.4. Multiangle Static Light Scattering (MASLS). The size distribution of spherical micelles and polymersomes was measured using an asymmetric flow field-flow fractionator (AFFFF) coupled in series to a 18-angle Dawn EOS MASLS photometer, equipped with a linearly polarized 30 mW gallium arsenide laser operating at 690 nm (Wyatt Technology Corp., Santa Barbara, CA). Light scattering spectra were analyzed using the ASTRA software (Wyatt Technology Corp.) to yield the hydrodynamic radius (R_h) and number-average mean radius (R_n). The mobile phase for all experiments was PBS at pH 7.3 filtered through 0.2 μm filters.

3. Results and Discussion

3.1. Morphology of Self-Assembled Colloids vs PB−PEO Molecular Weight. All observed morphologies were reproducibly imaged in two individual experimental batches. For each type of self-assembled structure, 20 images were collected and analyzed. A summary of morphologies observed for self-assembled PB−PEO colloids made by bulk rehydration and film rehydration probed using AFM is listed in Table 1. Three diblocks with different molecular weights, and similar hydrophilic weight fractions w_{PEO} (0.31−0.36) were investigated. As shown in Figure 1A−C, these self-assembled colloids displayed distinct morphologies ranging from spherical and wormlike micelles to polymersomes.

PB_{96}−PEO_{52} (subscript denotes the number of repeat units) colloids made by both bulk rehydration and film rehydration in PBS self-assembled into wormlike micelles. In contrast, PB_{219}−PEO_{121} colloids made by the two distinct preparation methods both self-assembled into polymersomes. However, PB_{407}−PEO_{286} colloids made by bulk rehydration self-assembled into compact ordered patterns of micelles, while PB_{407}−PEO_{286} colloids made by film rehydration self-assembled into polymersomes. The morphological details of different copolymer colloids will be discussed in further detail in sections 3.2 and 3.3.

The morphology of PB−PEO colloids with different degrees of polymerization of the PB block and different hydrophilic weight fractions of the PEO block was extensively studied using cryo-TEM.[24,25] However, the morphology of PB−PEO diblocks with larger hydrophobic core (molecular weights >20 kDa) has not been previously studied. According to the morphology diagram in Jain and Bates's study,[24,25] PB_{407}−PEO_{286} self-assembled colloids should exist as polymersomes. Our study shows that the morphology of PB_{407}−PEO_{286} colloids made by direct dissolution appears to be spherical micelles, which could be due to the extremely large molecular weight of the PB block. However, the morphology of PB_{407}−PEO_{286} colloids made by film rehydration exhibited closed bilayer structures (polymersomes). It is well-known that the morphology of self-assembled structures composed of amphiphilic block copolymers responds to changes in the molecular geometry, concentration of the amphiphile, and solvent.[38] It was suggested that dissolution of PB_{407}−PEO_{286} diblocks dispersed in an organic solvent and its subsequent rehydration in an aqueous solvent resulted in the transformation of the highly stretched hydrophobic chains and swollen hydrophilic chains to a more relaxed, entropically favored conformation.[39,40] This may have caused the morphology of PB−PEO self-assembled colloids to switch from micelles to polymer vesicles.[41] Hence, this may explain why self-assembled PB_{407}−PEO_{286} colloids prepared by film rehydration resulted in different morphologies compared to those made by bulk rehydration.

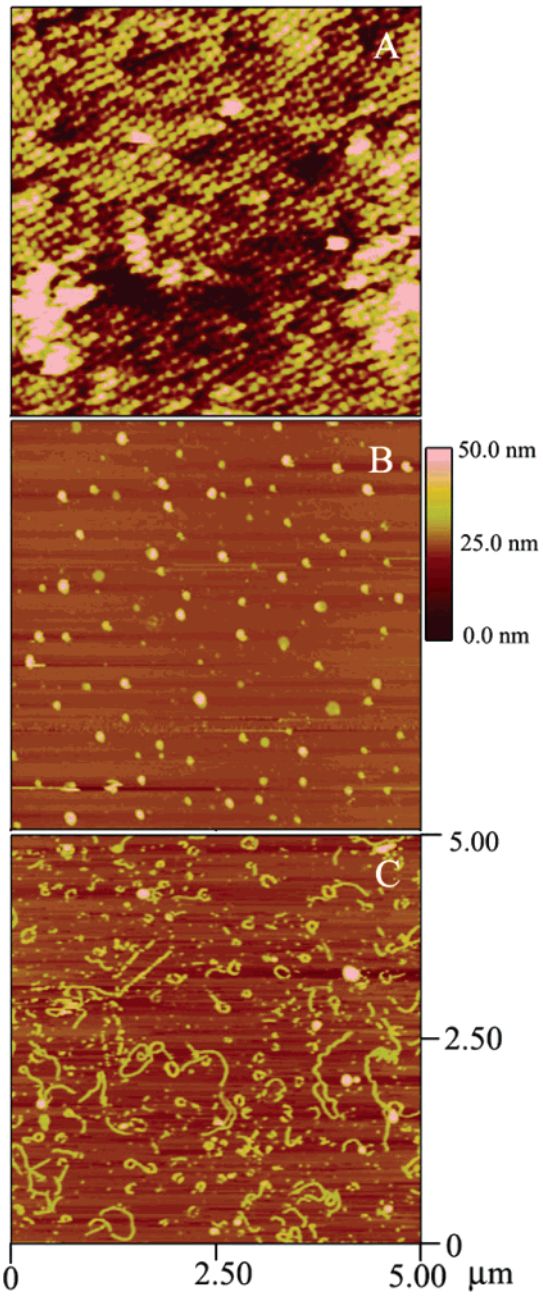

Figure 1. AFM fluid-tapping mode images capturing (A) PB_{407}−PEO_{286} micelles on glass, (B) PB_{219}−PEO_{121} polymersomes on mica, and (C) PB_{96}−PEO_{52} wormlike micelles on mica. Images were taken at 0.5 Hz and presented in height mode at a resolution of 512 × 512 pixels/line. The slow scan direction of each image was top to bottom, and the line scan direction was trace (right to left).

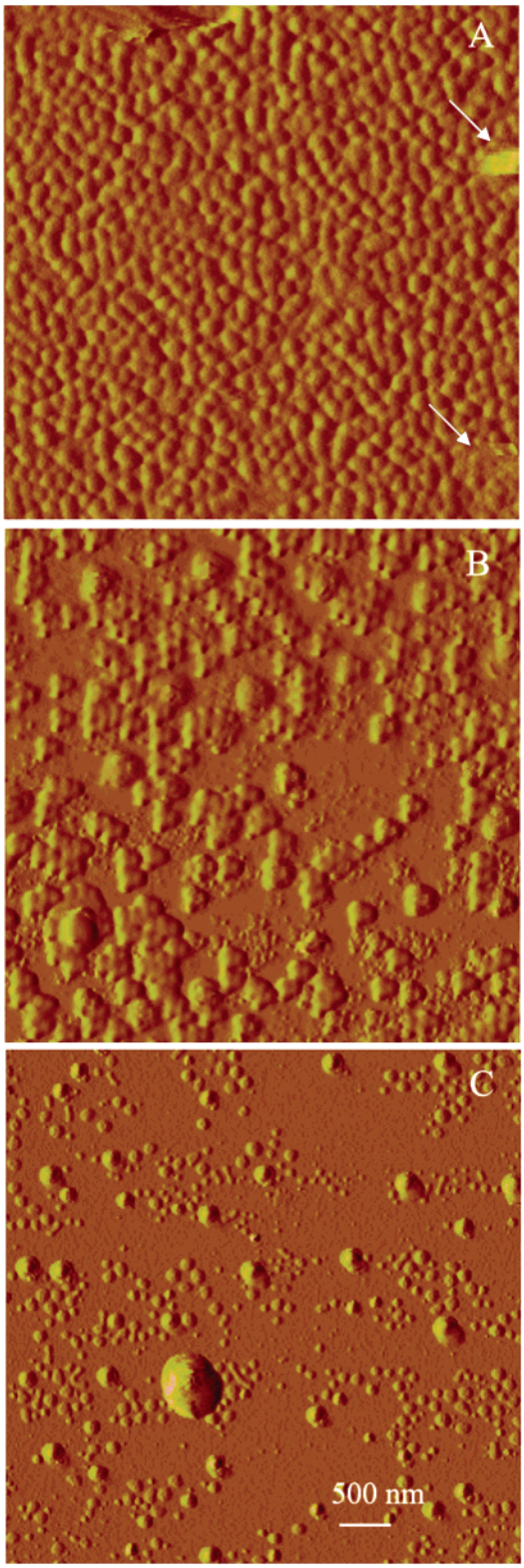

Figure 2. AFM fluid-tapping mode images capturing self-assembled PB_{407}−PEO_{286} colloids made by bulk rehydration: (A) on glass, adsorbed secondary layer marked with arrows; (B) on mica; and (C) on mica exposed to decreasing osmotic pressure by flushing deionized water through the fluid cell. Images were taken at 0.5 Hz and presented in amplitude mode at a resolution of 512 × 512 pixels/line. All images measured 5 μm × 5 μm. The slow scan direction of each image was top to bottom, and the line scan direction was trace (right to left).

3.2. Structure of Self-Assembled PB−PEO Spherical and Wormlike Micelles. Figure 2A shows the topography of PB_{407}−PEO_{286} self-assembled colloids prepared by bulk rehydration on glass slides. Upon absorption of 1 mg/mL of self-assembled PB_{407}−PEO_{286} onto clean glass, circular subunits arranged into semiregular arrays were clearly observed on the substrate surface, which implies formation of surface micelles.[21] These micelles have relatively clean and well-defined boundaries and pack compactly into semiregular dense arrays with very weakly adsorbed secondary layers beginning to form (marked with arrows). Since the initially absorbed polymer micelle layer screens further micelle absorption, the second layer absorbs onto the first polymer micelle layer very weakly. One can sweep away the larger aggregates settling down on top of the initial polymer micelle layers by increasing the imaging force. Since the AFM tip is only gently probing the top surface under AFM parameters optimized for imaging, discrete polymer micelles cannot be observed. Using a combination of on-line zoom and off-line section analysis tools (Figure 3A), gaps between clusters clearly indicate that the circular subunits are spherical diblock micelles absorbed on the substrate surface. Examining these semiregular arrays more closely, we found that these micelles are orderly arranged in hexagonally close packing order (see Figure 3A), with gaps isolating individual clusters. It is likely that the distortion (featured with some irregular clusters and gaps) of hexagonal packing is due to thermal drift of the scan area or more possibly due to the AFM probe physically sweeping away clusters. These micelles have similar heights and radii, which implies a high degree of homogeneity in the micelle dispersion. Specifically, absorbed micelles exhibited diameters of 105.6 ± 3.5 nm and heights of 8.0 ± 1.2 nm (n = 96, selected from 20 images). It should be noted here that the vertical height measured is much smaller than the measured radius. Here, it is proposed that once a micelle adsorbs onto the solid surface, the originally spherical copolymer micelle undergoes a structural change, which leads to spreading of the micelle across the substrate surface, which leaves only a micelle hemisphere protruding from the surrounding micelle layers.[19,42] Hence, the height measured is the height of the adsorbed micelle and not the height of the micelle in bulk solution. Similarly, the measured micelle diameter reflects the diameter of the adsorbed micelle and not its actual diameter in bulk solution. In addition, the radius of the micelle hemisphere measured by AFM is most likely overestimated due to convolutions between the AFM cantilever and the micelle hemisphere.[19] Hence, because of micelle adsorption and cantilever−micelle convolutions, the micelle radius and height measured by AFM do not reflect the true dimensions of micelles in bulk solution. The actual size of these micelles in bulk solution was characterized by multiangle static light scattering (MASLS) and measured 53.12 ± 0.05 nm in radius (Table 2). Interestingly, the experimentally observed micelle size is larger than that of an ordinary micelle (usually 20−60 nm in diameter), which could be attributed to the larger molecular weight (22 kDa) of the hydrophobic block.

The formation of lyotropic phases of amphiphilic PB−PEO in the concentration range between that of micellar solutions and the bulk phase (polymer gel) was previously observed using transmission electron microscopy (TEM).[38] In fact, the morphology of cross-linked PB−PEO gels exhibited cubic, hexagonal phases.[38,43,44] Highly ordered monolayers packed at the hexagonal level have

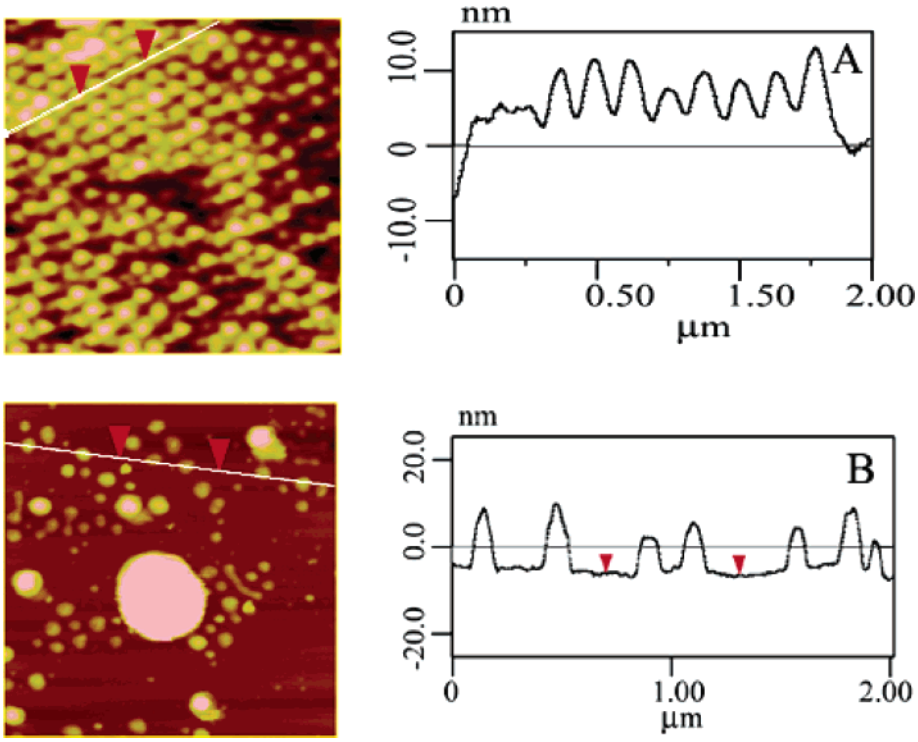

Figure 3. Off-line section analysis of a representative area of self-assembled $PB_{407}-PEO_{286}$ colloids made by bulk rehydration on (A) glass and (B) mica under osmotic swelling conditions (i.e., exposure to deionized water). The original scan of this image was captured in height mode, with a scan size of 2 μm × 2 μm, 0.5 Hz scan rate, top-to-bottom slow scan direction, trace (right to left) line scan direction, and at a resolution of 512 × 512 pixels/line.

Table 2. Hydrodynamic Radius and Number-Average Mean Radius of Self-Assembled PB−PEO Colloids Measured by Multiangle Static Light Scattering (MASLS)

	hydrodynamic radius, R_h (nm)		number-average mean radius, R_n (nm)	
diblock	bulk rehydration	film rehydration	bulk rehydration	film rehydration
$PB_{219}-PEO_{121}$	72.45 ± 0.13	67.19 ± 0.08	78.20 ± 0.03	71.20 ± 0.04
$PB_{407}-PEO_{286}$	53.12 ± 0.05	71.58 ± 0.11	50.32 ± 0.04	78.40 ± 0.05

been observed for charged micelles of poly(2-(dimethylamino)ethyl methacrylate)-*b*-poly(2-(diethylamino)ethyl methacrylate) (PDMA-*b*-PDEA) at lower micellar concentrations. In our study, we observed that neutral PB−PEO polymer micelles could also further self-assemble into ordered superstructures at lower micellar concentrations.

Adsorption of self-assembled $PB_{407}-PEO_{286}$ colloids at 1 mg/mL onto a more hydrophilic substrate, mica, was also investigated. As shown in Figure 2B, small clusters of aggregated micelles were highly absorbed on mica, which were not packed into ordered arrays. In addition, the surface density of micelles on mica was less than that observed on glass for a 1 mg/mL of diblock solution. We also investigated the effect of osmotic pressure on the topology of diblock micelles. Starting with highly absorbed micelle clusters on mica in PBS buffer, flushing deionized water through the AFM fluid cell leads to a decrease in ionic strength outside the micelles and osmotically swells them. As shown in Figure 2C, the original irregularly shaped aggregated cluster of micelles transformed into discrete regularly shaped spherical micelles with cleanly defined edges. After further on-line zoom in scanning and off-line section analyses, we can clearly see these features are discrete with complete spherical edges. The fact that we obtained different heights for individual micelles suggested that adsorption of the PEO corona onto mica is not homogeneous. These absorbed micelles have average diameters of 124.7 ± 3.6 nm and heights of 16.4 ± 4.2 nm (n = 96, selected from 20 images). The larger structures are probably polymersomes with apparent diameters of 219.6 ± 28.9 nm (n = 37, from a total 20 images). Therefore, self-assembled $PB_{407}-PEO_{286}$ colloids made by bulk rehydration possess only a small population of colloids with closed bilayer structure. Our results agree with those of Hamley et al.'s[20,21] study on poly(propylene oxide)-*b*-poly(ethylene oxide) diblock copolymer micelles adsorbed onto hydrophobic substrates (silica) and hydrophilic substrates (mica), in which $P_{94}E_{316}$ micelles arranged as compact semiregular arrays on silica, while at the same micelle concentration on mica, $P_{94}E_{316}$ micelles exhibited a discrete spherical morphology with well-defined edges.

It was observed that $PB_{96}-PEO_{52}$ self-assembled into wormlike micelles. Parts A and B of Figure 4 show self-assembled $PB_{96}-PEO_{52}$ colloids in PBS made by film rehydration and bulk rehydration, respectively. The wormlike micelles made by bulk rehydration (Figure 4B) exhibited a winding network with Y junctions at the ends, while micelles made by film rehydration (Figure 4A) arranged into spaghetti-like patterns. The network or spaghetti-like patterns indicated that the worm cylinders were arranged isotropically. Hexagonal packed lattices were not observed in our study due to the lower diblock copolymer concentrations utilized.[45] These adsorbed wormlike micelles measured 29.8 ± 4.3 nm in diameter and 10.3 ± 1.9 nm in height (n = 80, selected

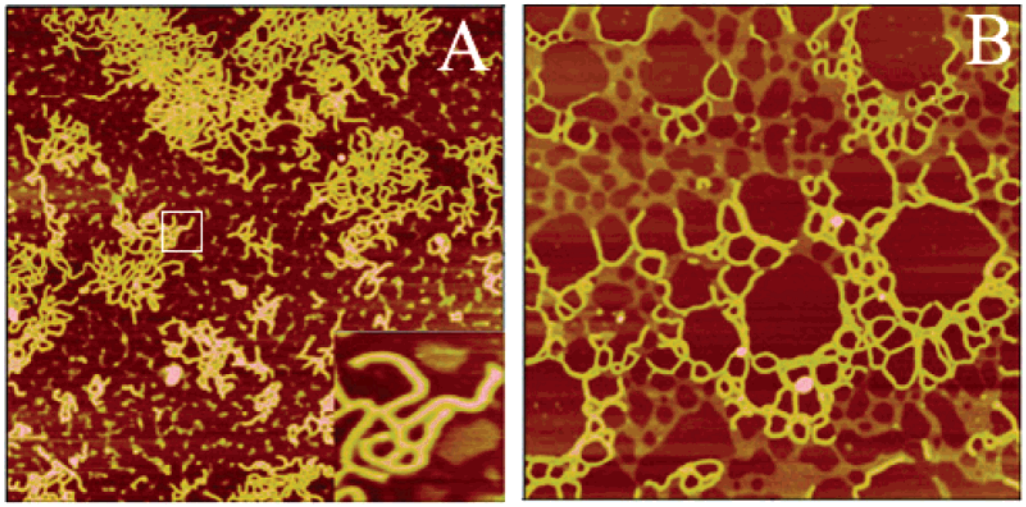

Figure 4. AFM fluid tapping mode images capturing self-assembled PB_{96}−PEO_{52} colloids made by (A) film rehydration and (B) bulk rehydration on mica. Images were taken at 0.5 Hz and presented in height mode with a resolution of 512 × 512 pixles/line. All images measured 5 μm × 5 μm and were captured at a 50 nm height scale. The slow scan direction of each image was top to bottom, and the line scan direction was trace (right to left). The inset in panel A is an on-line zoom-in image of the white boxed off area at a 500 nm × 500 nm scan size.

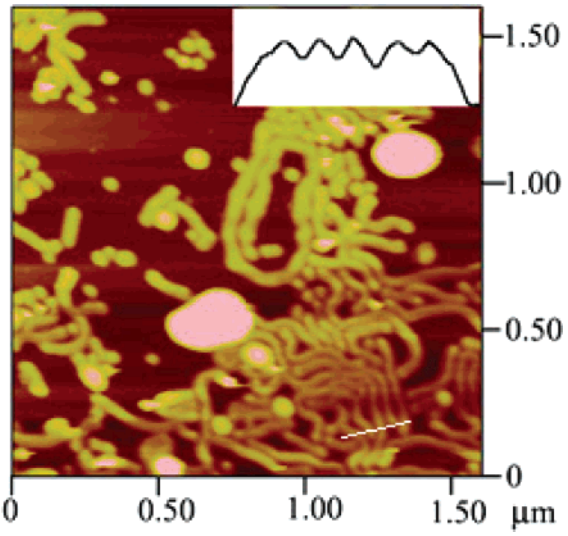

Figure 5. AFM fluid tapping mode images capturing self-assembled PB_{96}−PEO_{52} colloids made by bulk rehydration under osmotic swelling conditions (i.e., exposure to deionized water). The inset represents a section analysis of the white lined cross section. The image was taken at 0.5 Hz and presented in height mode at 50 nm height scale with a resolution of 512 × 512 pixels/line. The slow scan direction of each image was top to bottom, and the line scan direction was trace (right to left).

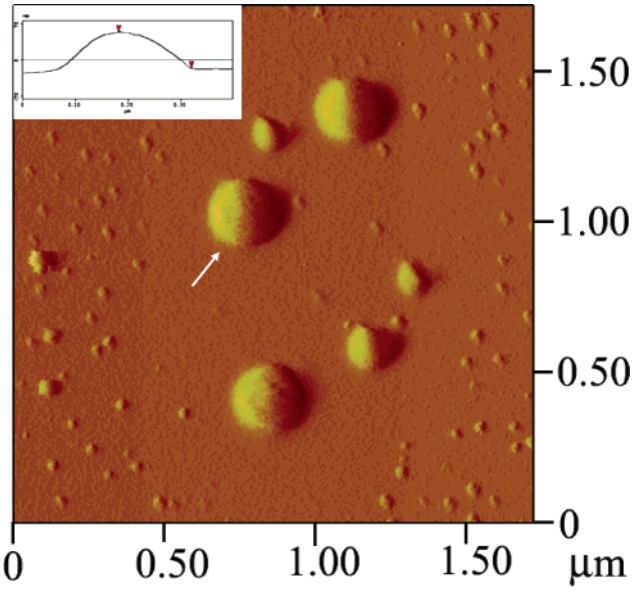

Figure 6. AFM fluid tapping mode images capturing self-assembled PB_{407}−PEO_{286} colloids made by bulk rehydration on mica. The inset represents a section analysis of the polymersome marked with an arrow. The image was taken at 0.5 Hz and presented in amplitude mode with a resolution of 512 × 512 pixels/line. The slow scan direction of each image was top to bottom, and the line scan direction was trace (right to left).

from 20 images). It was difficult to quantify the average length of these micelles since they were entangled together and formed network patterns. With AFM section analysis, we roughly estimated that these micelles were several micrometers in length. The formation of Y-junction and network patterns was most probably attributed to the high molecular weight of the hydrophobic block. Only a small population of polymer vesicles (n = 77 from a total of 40 images) coexisted with the wormlike micelles. Small worms as shown in Figure 1C might be due to the myriad of network fragments that are a result of vigorous agitation in the worm micelle formation process. The topology of wormlike micelles became sharper, when the osmotic pressure was decreased by switching the AFM imaging buffer from PBS to deionized water. This change caused the micelles to swell. Section analyses were conducted on multiple parallel micelles lying side-by-side (Figure 5, inset), and the broadening effect caused by the finite radius of the AFM tip was corrected as described by LaRue et al.[37] These adsorbed micelles measured 43.2 ± 2.8 nm in diameter and 17.5 ± 2.1 nm in height (n = 45, selected from 10 images), which implies that the wormlike micelles are swollen due to the osmotic gradient caused by the decreased ionic strength outside the micelles. When wormlike micelles were vigorously agitated, the network or spaghetti-like entangled micelles broke and re-formed into small cylinder-like micelles (see Figure 1C). Equilibration of the cylinder-like micelles transformed the initially cylindrical worms back into network patterns. A similar trend was ob-

Table 3. Apparent Diameter and Height of Self-Assembled PB−PEO Colloids Measured by AFM

	apparent diameter (nm)		height (nm)	
diblock	bulk rehydration	film rehydration	bulk rehydration	film rehydration
$PB_{96}-PEO_{52}$	34.3 ± 3.6	29.8 ± 4.3	14.2 ± 3.5	10.3 ± 1.9
$PB_{219}-PEO_{121}$	148.1 ± 8.7	123.8 ± 5.5	64.5 ± 4.2	62.4 ± 3.9
$PB_{407}-PEO_{286}$	105.6 ± 3.5	209.5 ± 8.6	8.0 ± 1.2	70.4 ± 3.1

served for poly(ethylene glycol)−poly(ethylethylene) (PEG−PEE) wormlike micelles by Dalhaimer et al.[26] using AFM, in which the contour length of several micron-long wormlike micelles was reduced to 1 ± 0.5 μm by brief intervals of sonication.

3.3. Structure of Self-Assembled PB−PEO Polymersomes. Representative images of self-assembled $PB_{407}-PEO_{286}$ colloids in PBS at 1 mg/mL prepared by film rehydration are shown in Figure 6. In contrast to the topology of self-assembled $PB_{407}-PEO_{286}$ colloids made by bulk rehydration, these vesicles are larger in diameter with clearly defined edges. Hence, discrete polymersomes were obtained. Section analysis of an individual polymersome (Figure 6, inset) revealed a hemispherical profile with an average diameter of 209.5 ± 8.6 nm and a height of 70.4 ± 3.1 nm (n = 107) (Table 3). The height measured by AFM is close to the hydrodynamic radius (71.58 ± 0.11 nm) measured by MASLS (Table 2). The apparent "shadow" associated with polymersomes on the image results from the relatively large height of polymersomes and the pyramid geometry of the AFM tip.[46] We exclude the possibility that larger features are micelles since we know from previous experience that micelles adsorbed onto mica surfaces in PBS exist as aggregated clusters composed of several small micelles.

The intermediate molecular weight diblock $PB_{219}-PEO_{121}$ (Figure 7A,B) possessed discrete spherical features, similar to self-assembled $PB_{407}-PEO_{286}$ colloids made by film rehydration. Section analysis (inset) revealed semicircular profiles with an average diameter of 148.1 ± 8.7 nm and height of 64.5 ± 4.2 nm (n = 128) for colloids made by bulk rehydration. The colloids made by film rehydration possess an average diameter of 123.8 ± 5.5 nm and height of 62.4 ± 3.9 nm (n = 128) (Table 3). The heights of these vesicles are close to the hydrodynamic radii measured by MASLS in bulk solution (Table 2). The morphology of $PB_{219}-PEO_{121}$ polymer vesicles agrees well with the experimentally measured morphology diagram in Jain and Bates's study.[24]

Interestingly, $PB_{407}-PEO_{286}$ polymersomes were highly nonuniform compared to $PB_{219}-PEO_{121}$ polymersomes imaged on mica. We hypothesize that the heterogeneity of polymersomes on mica resulted from weaker interactions between the hydrophilic brush and the hydrophilic mica substrate. Because of the longer hydrophilic brush of $PB_{407}-PEO_{286}$ vs $PB_{219}-PEO_{121}$, the interaction between $PB_{407}-PEO_{286}$ polymersomes and the mica substrate is probably weaker compared to $PB_{219}-PEO_{121}$ polymersomes. Hence, $PB_{407}-PEO_{286}$ polymersomes were more prone to be swept away by the AFM tip, which resulted in nonuniform patterns of polymersomes being deposited on the mica substrate. A similar trend was also observed for $PB_{407}-PEO_{286}$ micelles on mica (Figure 2C), which was relatively nonuniform compared with the $P_{94}E_{316}$ micelles imaged on mica in Hamley's study.[21] The longer hydrophilic brush of $PB_{407}-PEO_{286}$ (higher M_w compared to $P_{94}E_{316}$), and hence its weaker interaction with the mica substrate probably resulted in the observed heterogeneity of $PB_{407}-PEO_{286}$ micelles on mica.

Cryo-TEM has been widely used to study polymersome structure.[10,11] To the best of our knowledge, no previous work on polymersomes have been made using AFM in aqueous solution. Cryo-TEM allows real-space imaging of self-assembled colloids at high resolution. However, during sample preparation, solution flow and shear stress in the blotting process favor formation of nonequilibrium structures by breaking and re-forming the self-assembled structures.[23] The need for the complicated blotting process and vitrification of samples for Cryo-TEM imaging is negated by AFM imaging, which measures the 3-D structure of colloids equilibrated under physiological conditions. In this manner, the self-assembled structures probed by AFM should be close to the native structure observed in vivo.[47]

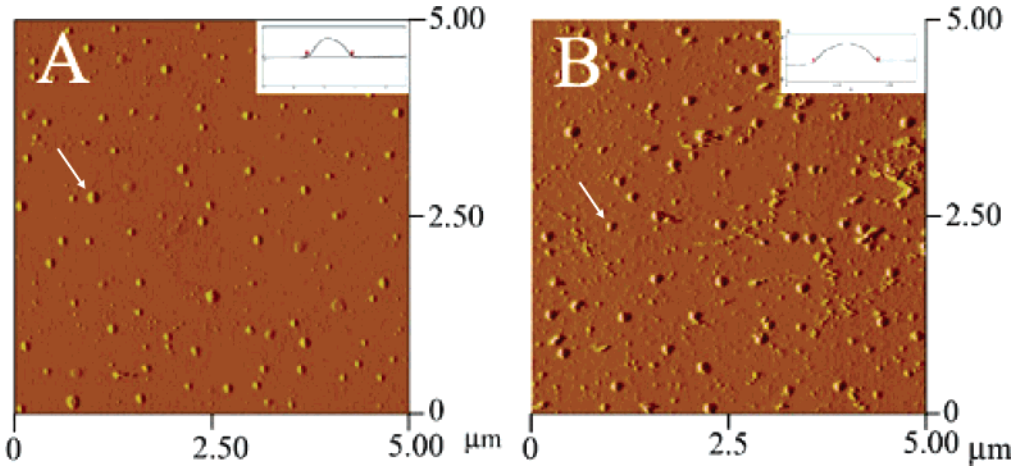

Figure 7. AFM fluid tapping mode images capturing self-assembled $PB_{219}-PEO_{121}$ colloids made by (A) bulk rehydration and (B) film rehydration on mica. Images were taken at 0.5 Hz and presented in amplitude mode with a resolution of 512 × 512 pixels/line. All images measured 5 μm × 5 μm. The slow scan direction of each image was top to bottom, and the line scan direction was trace (right to left). Insets represent section analyses of vesicles marked with arrows.

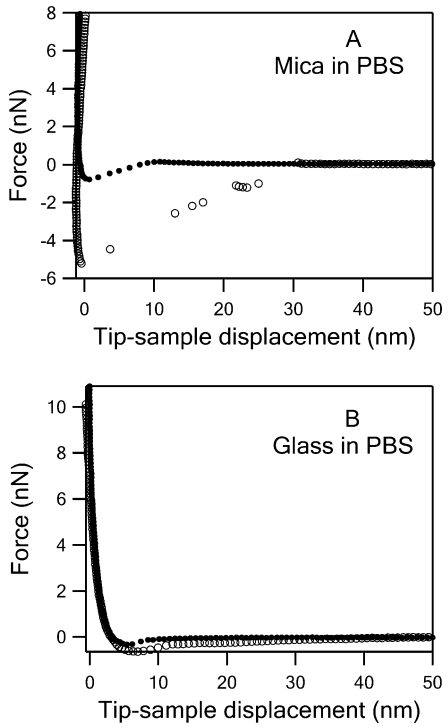

Figure 8. Typical force−distance curves on (A) mica and (B) glass in PBS buffer. The dotted curves were recorded on approach of the AFM tip, and circular dotted curves were obtained on retraction of the AFM tip.

3.4. AFM Force Measurements on Spherical PB−PEO Micelles. Force studies were carried out on self-assembled PB_{407}−PEO_{286} and PB_{96}−PEO_{52} colloids prepared by both bulk rehydration and film rehydration. *Z*-axis piezo extension vs cantilever deflection profiles were recorded and later converted to force vs tip−sample displacement curves. As a control, force−distance profiles taken on bare mica and glass in PBS are shown in Figure 8A,B. Similar to previous studies,[42,48] van der Waals attractive forces occur at 8.3 ± 1.1 nm away from the substrate surface. No appreciable long-range repulsive forces were observed for force curves obtained on mica. van der Waals attraction becomes the most dominant force observed, since higher electrolyte concentrations in PBS screen the electrostatic repulsion between surfaces.[49] Force curves on glass in PBS (Figure 8B) showed no appreciable repulsion and only a weak attraction at separations of 6.7 ± 2.2 nm.

Figure 9A−C shows representative force curves of PB_{407}−PEO_{286} micelles adsorbed onto glass at different times. On examination, all self-assembled diblock structures withstood an AFM tip loading force of ∼7 nN without undergoing irreversible structural changes. After every 30 cycles of extension and retraction, the topography was recorded to ensure that the self-assembled structures remained intact. When the AFM tip approached the polymer micelles, substantial repulsion of the tip occurred at 110.2 ± 8.9 nm (averaged from 73 force curves), which is close to the hydrodynamic diameter of the micelles. The strong repulsion is mainly derived from the dense PEO corona of the polymer micelles, since long-range electrostatic repulsive forces are negligible in our studies. Because of thermally driven Brownian motion, PEO brushes exert repulsive forces arising from reduction of the polymer's entropy as the AFM tip moves through their occupied space.[50] As micelles are further compressed by the AFM tip, a sharp downward deflection, known as the "escape transition", appears on the approaching portion of the force curves (Figure 9A,B) at 47.7 ± 12.8 nm from the substrate surface and results in a force peak of 1.95 ± 0.32 nN ($n = 57$). The gap associated with the downward deflection has a width of 25.3 ± 7.9 nm ($n = 57$), which is much larger than the "punch through" gap typically observed for force curves of liposomes or a surfactant covered surface (∼5 nm).[42,50] In Figure 9A, following the sharp "escape transition", a small discontinuity was present at 15.2 ± 9.6 nm, which resulted in a force of 1.73 ± 0.52 nN ($n = 33$). This second escape transition is much more clearly shown in Figure 9B, with a sharp force peak at 17.9 ± 7.4 nm and compression force of 2.31 ± 0.36 nN ($n = 24$), and manifests itself as a narrow sharp downward deflection on the force curves. After probing the micelles for ∼40 min, the force curves become smoother for most of the recorded force curves ($n = 12$), while some force curves ($n = 4$) exhibited a small discontinuity at 54.3 ± 18.5 nm with a force of 2.9 ± 0.4 nN, which probably results from the slight lateral movement of the AFM tip or micelles.

It is well-known that under a critical compression force polymer chains partially escape from under the approaching compression obstacle.[27,28,51,52] When the AFM tip compresses micelles weakly, the hydrophilic chain does not "see" the edge of the AFM tip, so it deforms uniformly, and the force that the chain imposes on the AFM tip grows exponentially as predicted theoretically.[50] Figure 9A inset shows experimental force vs distance curve fitting ($R^2 = 0.986$) to the exponentially decaying function $F = Ae^{-D/\lambda}$, where the amplitude A and decay length λ are regression parameters. This exponentially decaying function was derived from the Alexander de Gennes equation describing the forces acting between two surfaces bearing polymer brushes in a good solvent.[53] In the case of only one surface and no strong adsorption between the polymer brushes and AFM tip, the force per unit area between the AFM tip and PEO brushes could be approximated by[54] $f \approx 50k_BT\Gamma^{3/2}e^{-2\pi D/L_0}$. To account for the shape of the AFM tip, the approximate force on the tip is[54] $F \approx 50\pi k_BTR\Gamma^{3/2}e^{-2\pi D/L_0}$,where R is the radius of the tip end, L_0 is the equilibrium length of the polymer brushes, k_B is Boltzmann's constant, T is the absolute temperature, Γ is the adsorption density in m^{-2}, and D is the distance between the two surfaces. After fitting the repulsive force to the exponentially decaying function, an average decay length $\lambda = L_0/2\pi = 20 \pm 7$ nm and an amplitude of 1.98 ± 0.15 nN ($n = 10$) were regressed. On the basis of the degree of polymerization of the PEO block and the segment length of a PEO monomer (σ = 0.35 nm),[55] a contour length of 100.1 nm was calculated for the PEO block. From the regressed decay length, the equilibrium length of the PEO brush, $L_0 = 125.6$ nm, was obtained, which is close to the contour length of the PEO brush (in the fully stretched state) and larger than the corona thickness of the micelles (in the relaxed state). This discrepancy arises from the fact that hydrophilic PEO brushes are not strictly immobilized by the micelle hydrophobic core. Hence, polymer chains are not simply being compressed as described by the Alexander de Gennes equation, in which polymer chain bending was neglected. The polydispersity of the PEO block may also account for the large errors in calculating L_0, since the longer polymer brushes would establish

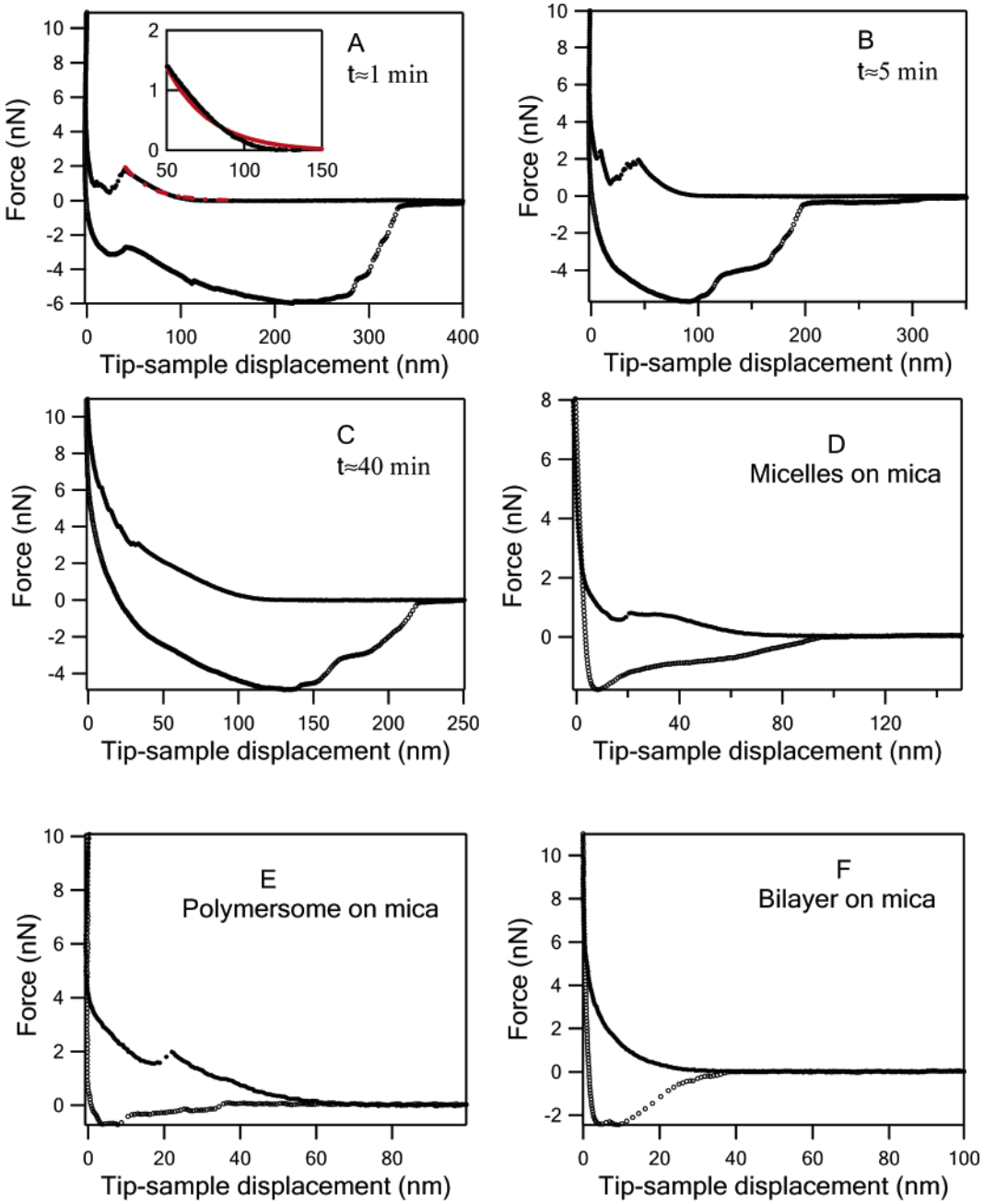

Figure 9. Typical force−sample separation curves obtained on different self-assembled PB_{407}−PEO_{286} colloids. PB_{407}−PEO_{286} micelles on glass at 1, 5, and 40 min are shown in (A)−(C), respectively. PB_{407}−PEO_{286} micelles on mica (D), PB_{407}−PEO_{286} polymersomes (E), and PB_{407}−PEO_{286} double bilayer (F). The dotted curves were recorded on approach of the AFM tip, and circular dotted curves were obtained on retraction of the AFM tip. Inset of (A) shows nonlinear least-squares fitting (red) of the approaching repulsive portion of the force curve (black) to the Alexander de Gennes force model, $F \approx 50\pi k_B T R \Gamma^{3/2} e^{-2\pi D/L_0}$ ($R^2 = 0.986$).

contact with the AFM tip first and subsequently result in repulsive forces. Nonetheless, this simplistic exponential decay model does qualitatively describe the steric repulsion driven by thermal motion of the polymer brushes as the AFM tip compresses the polymer micelles.

However, at an applied critical compression force the polymer chain can reduce its energy by partially escaping from under the approaching AFM tip. Several simulations[27,28,52] have confirmed the existence of the escape transition; however, a sharp downward deflection in the force curves caused by the "escape transition" has not been observed experimentally in AFM contact mode to the best of our knowledge. The challenge of observing the escape transition in practice stems from the difficulty in approaching the grafted chain "head on" and controlling the necessary ideal geometry, which consists of end-grafted polymer chains with a random coil conformation confined between two flat repulsive surfaces. In the case of an individual PB_{407}−PEO_{286} micelle, the hydrophilic PEO brush layer is "fixed" to the PB hydrophobic core, and the lateral motion of micelles on the substrate surface was constrained by the close-packed arrangement, which mimics the conformation of a grafted polymer chain tethered onto a substrate. According to Guffond et al.'s study,[28] for PEO chains end tethered onto substrates with polymerization degrees similar to PEO blocks in our study, the first escape transition occurred at 0.19 nm, which is beyond the accuracy of our AFM. Besides, at that separation, short-

range repulsive forces become dominant. This might be the main reason why the transition escape has not been observed using AFM on end-grafted polymer chains.

Small discontinuities in the force curve were referred to as "escape transitions" by Hamley et al.[21] for block copolymer micelles using AFM in Tapping Mode. The authors reported that the "small jump or discontinuity" is analogous to an "escape transition." Because of the smaller molecular weight of $P_{94}E_{316}$ and hence shorter hydrophilic corona length of the resulting micelles, escape transitions occurred at ~2−3 nm, very close to the substrate surface. Therefore, no clearly defined sharp "escape transition" was reported. In comparison, our study clearly shows the distinct "escape transition" as the AFM tip compresses the hydrophilic corona of the diblock copolymer micelles at a critical applied force of 1.95 ± 0.32 nN.

Hence, two "escape transitions" were observed on force curves of PB_{407}−PEO_{286} micelles (Figure 9B) at an applied force of 1.95 ± 0.32 nN and 2.31 ± 0.36 nN, which confirms Ennis and Sevick's[27] theoretical prediction that diblock copolymers can exhibit multiple escape transitions. We presume that the first escape transition is associated with the partial expulsion of the hydrophilic PEO block away from the AFM tip; the second escape transition occurs at higher compressions where the hydrophobic PB block begins to stretch and change conformation. Discher and co-workers[56] observed that the hydrophobic core thickness displayed a power-law dependence: $d = \Phi(MW_{phob})^{\zeta}$, where $\zeta = {}^1/_2$, MW_{phob} is the molecular weight of the hydrophobic moiety, and Φ is a constant. On the basis of this dependence, the hydrophobic core thickness is estimated to be 27.4 nm. In addition, on the basis of the hydrodynamic radius of the PB_{407}−PEO_{286} micelle (53.12 ± 0.05 nm), the length of the hydrophilic brush is estimated to be 26 nm. The distance difference between the two escape transitions (47.7 nm − 17.9 nm = 30 nm) is close to the length of the hydrophilic brush, which implies that the two escape transitions probably correspond to conformational changes of the hydrophilic corona and hydrophobic core.

Downward deflections in the approaching portion of force curves have been observed by Webber et al.[19,57] in their study on positively charged micelles of poly(2-(dimethylamino)ethyl methacrylate)-*b*-(2-(diethylamino)ethyl methacrylate) (PDMA−DEA). In their studies, the force curves were further complicated by long-range electrostatic repulsion between positively charged micelles of PDMA−DEA and the AFM tip. The downward deflection observed in their studies was mainly ascribed to the tip punching through the hydrophobic core of the micelles. However, if this is the case, the second small downward deflection would not occur given the fact that once the AFM tip contacts the mica surface, strong repulsive forces will monotonically increase. Therefore, we concluded that the downward deflection present in our force curves of PB−PEO micelles resulted from escape transitions of the block polymer chains.

The retracting portion of the force curves on PB_{407}−PEO_{286} micelles exhibited pronounced hysteresis and showed a markedly broad region of attraction. A strong adhesion force of 5.33 ± 1.56 nN ($n = 73$) was detected between the AFM tip and polymer micelles. Beyond the maximum adhesion force, the retracting curves typically exhibited multiple jumps (Figure 9B,C), which suggest that multiple attachment points associated with the high molecular weight polymer detach slowly in a successive manner from the AFM tip. As the AFM tip moves away from the substrate, the coiled PEO brushes detach from the AFM tip until they are pulled out of the PEO brush region, and an attractive force develops on the tip. The broad region of the retraction curves (228 ± 45 nm, $n = 73$) is also related to the adhesion between the entangled hydrophilic PEO block of the diblock polymer and the AFM tip. No such broad regions of the retraction curves were observed in Hamley et al.'s study.[20,21] We attribute this feature to the markedly long chains of PEO in our diblock copolymers (100.1 nm in contour length), which are prone to interact favorably with the AFM tip.

AFM force imaging of the same micelles on mica showed different force curve profiles (Figure 9D). A strong repulsion was observed at 82.5 ± 11.2 nm and increased almost linearly from 61.0 ± 13.4 nm and then flattened out at 38.7 ± 8.5 nm ($n = 15$). The linear springlike response of the force curve from a 61.0 ± 13.4 nm separation is perhaps indicative of hydrophobic core compressions. A jump-in event (escape transition) occurs at 21.5 ± 9.2 nm and an applied force of 0.81 ± 0.12 nN, where the hydrophilic PEO block probably changed conformation as the AFM tip passed through the hydrophobic micelle core and then continued its way through the dense hydrophilic corona of the micelle. The flat region and following "jump-in" event of these force curves could also be attributed to the lateral motion of the micelles, as the micelles were only loosely tethered to the mica surface by the hydrophilic brush.

It is interesting to note that two escape transitions were observed for PB_{407}−PEO_{286} micelles on glass substrates, while only one escape transition was observed for PB_{407}−PEO_{286} micelles on mica substrates. We ascribe this behavior to the weaker interaction between mica and the self-assembled colloid compared to that between the self-assembled colloid and the glass substrate. In the case of micelles on mica, micelles were only tethered by the hydrophilic brush to the hydrophilic mica substrate and hence were mobile on the substrate surface. Conversely, in the case of micelles on glass, the micelles were strongly adsorbed to the relatively hydrophobic glass surface, with the hydrophobic core in contact with the glass substrate surface. As shown in Figure 11, as the AFM tip probes the micelles on glass, because of strong adsorption of the hydrophobic core onto the glass surface, it is possible for the AFM tip to probe whole micelles (Figure 11A) in a cycle of extension and retraction. Therefore, two escape transitions were observed. However, as the AFM tip compresses micelles on mica, because of the much weaker interaction between the hydrophilic brush and mica substrate, the lateral motion of the micelles on mica may cause the AFM tip to only probe the hydrophilic brush layer (Figure 11B) or slip off the micelle hydrophobic core and probe the hydrophilic brush layer on its way down to the substrate surface (Figure 11C). Therefore, only one escape transition corresponding to the hydrophilic brush conformation change was observed.

The surface roughness of fresh cleaved mica and clean glass coverslips was measured to be 0.042 and 0.179 nm, respectively. Surface roughness may partially contribute to the AFM force measurement. We hypothesize that nanoscale irregularities at a hydrophobic surface probably facilitate the adsorption of the hydrophobic core onto the glass substrate,[58] which resulted in a larger

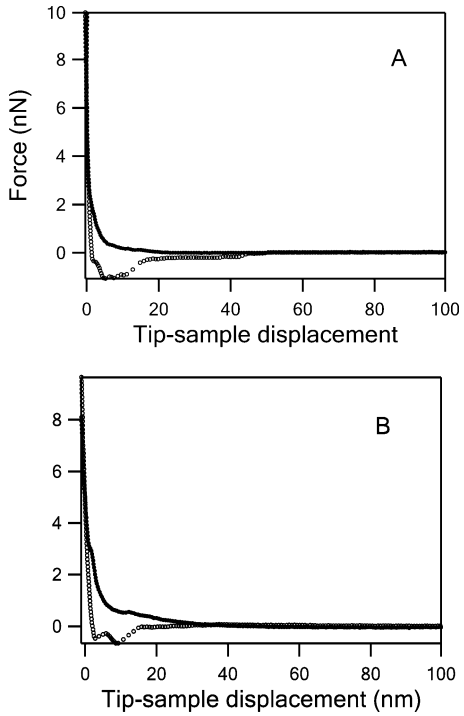

Figure 10. Typical force−sample separation curves of self-assembled PB_{96}−PEO_{52} wormlike micelles made by (A) bulk rehydration and (B) film rehydration. The dotted curves were recorded on approach of the AFM tip, and circular dotted curves were obtained on retraction of the AFM tip.

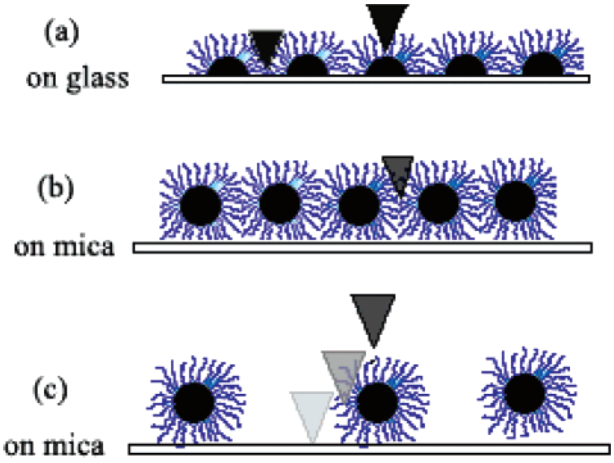

Figure 11. Adsorption of PB_{407}−PEO_{286} micelles on glass and mica substrates at 1 mg/mL of diblock copolymer. Gray triangles represent the location of the AFM tip: (a) on glass, micelles are fully absorbed and the AFM tip probes whole micelles; (b) on mica, micelles are tethered to the mica substrate by the hydrophilic brush, in this case the AFM tip passes through the hydrophilic corona on its way to the substrate surface without contacting the hydrophobic core; (c) on mica, the AFM tip slips off the hydrophobic core and then passes through the hydrophilic corona until it contacts the substrate surface.

surface micelle density on the glass surface. Hence, the AFM tip could probe whole micelles, which probably resulted in the observation of two escape transitions. On the basis of the results presented so far, the effect of surface roughness on force measurements needs to be investigated further.

3.5. AFM Force Measurements on Polymersomes and Wormlike Micelles. On the basis of the surface tension γ, the pressure difference across the membrane of a polymersome can be estimated according to Laplace's equation $\Delta p = 2\gamma/R$, where R is the radius of the polymersome. In the case of PB_{407}−PEO_{286} polymersomes, with an average hydrodynamic radius of 78.4 nm and $\gamma = 25$ pN/nm as a typical interfacial tension for the present block copolymer colloids,[59] an upper value of 12.3 nN was estimated for the loading force ($F = 2\pi R\gamma$) necessary to rupture the vesicle. Hence, application of external forces <12.3 nN will enable the internal pressure within intact vesicles to resist AFM tip compression. Therefore, at a loading force of ~7 nN, the polymersomes remained intact. Topography imaging after force probing confirmed the fact that the polymersomes (not shown) remained unruptured at the present applied loading force.

Force curves of PB_{407}−PEO_{286} polymersomes made by film rehydration are shown in Figure 9E (in tapping mode) and Figure 9F (in contact mode). Appreciable repulsion at 64.3 ± 11.9 nm resulting from compression of the hydrophilic corona was detected. At an applied force of 2.0 ± 0.3 nN and 22.5 ± 8.1 nm ($n = 7$) separation from the substrate surface (Figure 9E), a "jump-in" event with a gap 7.3 ± 2.5 nm occurred on the approaching curves. Previous studies[35,42] of force curves obtained on liposomes showed that the "jump-in" event occurs as the probe abruptly penetrates the lipid bilayer. Similarly, the "jump-in" event on the force curve of polymersomes probably implies that the AFM tip broke through the polymersome's bilayer. At a tip−substrate separation of 18.4 ± 3.2 nm ($n = 7$), the force curve exhibits an almost linear springlike response, which implies that the hydrophobic core of the polymersome bilayer is compressed. The hydrophobic bilayer has a height of ~18 nm, which is close to the hydrophobic core thickness of micelles formed with a similar diblock copolymer.[11]

Figure 9F represents another type of typical force curve observed for an individual polymersome in contact mode. Without the presence of a downward deflection, the approaching curve follows the classic exponential increase from approximately 38.9 ± 5.3 nm above the mica surface ($n = 10$). In this case, we presumed the polymersomes formed into a double bilayer patch due to the strong friction caused by the AFM tip scanning in contact mode. This may have caused the aqueous core of the polymersomes to be squeezed by the AFM tip in contact mode, which consequently lead to deformation of adsorbed polymersomes into double bilayer patches. While liposome bilayers are usually ruptured under 1−2 nN of loading force,[35,42] the polymersome bilayer remained intact at ~7 nN applied force before rupture. This suggests that polymersomes could sustain higher loading forces due to the thicker hydrophobic core (~20 nm) vs liposomes (~4 nm). The adhesion force between polymersomes and the AFM tip was 0.64 ± 0.29 nN in tapping mode and 2.09 ± 0.68 nN in contact mode, which are both less than the observed adhesion force between polymer micelles and the AFM tip (5.33 ± 1.56 nN). We hypothesize the dual presence of a less adhesive force and a smaller broad attractive region of retracting force curves is probably due to the larger curvature of micelles and higher density of the hydrophilic corona on the surface of micelles. Therefore, as the AFM tip is pulled out of the micelle's hydrophilic corona, stronger adhesive forces develop on the AFM tip.

Parts A and B of Figure 10 show the force curve profiles of PB_{96}−PEO_{52} wormlike micelles prepared by

bulk rehydration and film rehydration, respectively. Generally, the AFM tip experiences appreciable repulsion at a separation of 35.3 ± 5.8 nm (n = 37) and monotonically increases until the AFM tip makes contact with the substrate surface. No downward deflection was observed on the approaching portion of both force curves. However, force curves on wormlike micelles prepared by film rehydration (Figure 10B) shows a discontinuity at 10 ± 4 nm (n = 20), which probably is indicative of a conformational change in the PEO block at a loading force of 0.85 ± 0.12 nN or the lateral movement of micelles under the AFM tip. The retracting portion of the force curves both show two adhesion peaks. The highest adhesion force was measured at 1.05 ± 0.38 nN (n = 17) and 0.76 ± 0.24 nN (n = 20) for wormlike micelles made by bulk rehydration and film rehydration, respectively. The saw-tooth-like attractive force profiles are indicative of the existence of multiple attachment points between polymer chains and the AFM tip. Thus, as multiple hydrophilic chains are being sequentially pulled off during tip retraction, adhesive forces develop on the AFM tip. In comparison with $PB_{407}-PEO_{286}$ micelles, $PB_{96}-PEO_{52}$ wormlike micelle force profiles showed both weaker repulsive forces and adhesive forces, which is a direct consequence of the shorter hydrophilic block of $PB_{96}-PEO_{52}$ diblocks.

4. Conclusions

The structures of self-assembled PB−PEO colloids made by bulk and film rehydration were probed in aqueous solution using AFM in Tapping Mode. Three PB−PEO copolymers with different degrees of polymerization exhibited self-assembled colloidal structures, ranging from spherical micelles, to wormlike micelles, to polymersomes. Semiregular arrays of hexagonally packed PB−PEO micelles were observed at 1 mg/mL of diblock copolymer. Isotropic wormlike micelle networks were evident for PB−PEO diblocks with lower molecular weights. Force curve measurements on compact micelles on glass substrates showed two sharp downward deflections on the approaching force curves, which implied the presence of two "escape transitions". These two escape transitions probably correspond to conformational changes of the hydrophilic corona and hydrophobic core upon approaching AFM tip compression of the micelles. The retracting portion of the force curves exhibited a broad region of attractive force and multiple peaks, which implies the presence of multiple attachment points of coiled PEO hydrophilic blocks to the AFM tip. Taken together the results of this study shed new light on the structure and mechanical response of self-assembled PB−PEO colloids as a function of copolymer composition and method of preparation.

Acknowledgment. We thank Fei Liu at the University of Notre Dame for helpful discussions about AFM force measurement. We also acknowledge support from the National Science Foundation BES-0196432.

References and Notes

(1) Allen, T. M.; Cullis, P. R. *Science* **2004**, *303*, 1818−1822.
(2) Lasic, D. D. *J. Controlled Release* **1997**, *48*, 203−222.
(3) Lasic, D. D.; Martin, F. *Stealth Liposomes*; CRC Press: Boca Raton, FL, 1995.
(4) Hubbell, J. A. *Science* **2003**, *300*, 595−596.
(5) Savic, R.; Luo, L.; Eisenberg, A.; Maysinger, D. *Science* **2003**, *300*, 615−618.
(6) Forster, S.; Konrad, M. *J. Mater. Chem.* **2003**, *13*, 2671−2688.
(7) Discher, D. E.; Eisenberg, A. *Science* **2002**, *2002*, 967−973.
(8) Antonietti, M.; Forster, S. *Adv. Mater.* **2003**, *15*, 1323−1333.
(9) Discher, B. M.; Hammer, D. A.; Bates, F. S.; Discher, D. E. *Curr. Opin. Colloid Interface Sci.* **2000**, *5*, 125−131.
(10) Discher, B. M.; Won, Y.; Ege, D. S.; Lee, J. C.; Bates, F. S.; Discher, D. E.; Hammer, D. A. *Science* **1999**, *284*, 1143−1146.
(11) Bermudez, H.; Brannan, A. K.; Hammer, D. A.; Bates, F. S.; Discher, D. E. *Macromolecules* **2002**, *35*, 8203−8208.
(12) Photos, P. J.; Bacakova, L.; Discher, B.; Bates, F. S.; Discher, D. E. *J. Controlled Release* **2003**, *90*, 323−334.
(13) Shimada, K.; Matsuo, S.; Sadzuka, Y.; Miyagishima, A.; Nozawa, Y.; Hirota, S.; Sonobe, T. *Int. J. Pharm.* **2000**, *203*, 255−263.
(14) BeduAddo, F. K.; Tang, P.; Xu, Y.; Huang, L. *Pharm. Res.* **1996**, *13*, 710−717.
(15) Spatz, J. P.; Mossmer, S.; Hartmann, C.; Moller, M.; Herzog, T.; Krieger, M.; Boyen, H. G.; Ziemann, P.; Kabius, B. *Langmuir* **2000**, *16*, 407−415.
(16) Spatz, J. P.; Sheiko, S.; Moller, M. *Macromolecules* **1996**, *29*, 3220−3226.
(17) Meiners, J. C.; Ritzi, A.; Rafailovich, M. H.; Sokolov, J.; Mlynek, J.; Krausch, G. *Appl. Phys. A: Mater. Sci. Process.* **1995**, *61*, 519−524.
(18) Regenbrecht, M.; Akari, S.; Forster, S.; Mohwald, H. *J. Phys. Chem. B* **1999**, *103*, 6669−6675.
(19) Webber, G. B.; Wanless, E. J.; Armes, S. P.; Baines, F. L.; Biggs, S. *Langmuir* **2001**, *17*, 5551−5561.
(20) Connell, S. D.; Collins, S.; Fundin, J.; Yang, Z.; Hamley, I. W. *Langmuir* **2003**, *19*, 10449−10453.
(21) Hamley, I. W.; Connell, S. D.; Collins, S. *Macromolecules* **2004**, *37*, 5337−5351.
(22) Allen, C.; Maysinger, D.; Eisenberg, A. *Colloids Surf. B* **1999**, *16*, 3−27.
(23) Horber, J. K. H.; Miles, M. J. *Science* **2003**, *302*, 1002−1005.
(24) Jain, S.; Bates, F. S. *Macromolecules* **2004**, *37*, 1511−1523.
(25) Jain, S.; Bates, F. S. *Science* **2003**, *300*, 460−464.
(26) Dalhaimer, P.; Engler, A. J.; Parthasarathy, R.; Discher, D. E. *Biomacromolecules* **2004**, *5*, 1714−1719.
(27) Ennis, J.; Sevick, E. M. *Macromolecules* **2001**, *34*, 1908−1916.
(28) Guffond, M. C.; Williams, D. R. M.; Sevick, E. M. *Langmuir* **1997**, *13*, 5691−5696.
(29) Lee, J. C.; Bermudez, H.; Discher, B. M.; Sheehan, M. A.; Won, Y.; Bates, F. S.; Discher, D. E. *Biotechnol. Bioeng.* **2001**, *73*, 135−145.
(30) Li, S.; Palmer, A. F. *Langmuir* **2004**, *20*, 4629−4639.
(31) Li, S.; Palmer, A. F. *Langmuir* **2004**, *20*, 7917−7925.
(32) Nickels, J.; Palmer, A. F. *Langmuir* **2003**, *19*, 10581−10587.
(33) Palmer, A. F.; Wingert, P.; Nickels, J. *Biophys. J.* **2003**, *85*, 1233−1247.
(34) Magonov, S. N.; Elings, V.; Whangbo, M. H. *Surf. Sci.* **1997**, *375*, L385−L391.
(35) Schneider, J.; Dufrene, Y. F.; Barger Jr., W. R.; Lee, G. U. *Biophys. J.* **2000**, *79*, 1107−1118.
(36) Dufrene, Y. F.; Lee, G. U. *Biochim. Biophys. Acta* **2000**, *1509*, 14−41.
(37) LaRue, I.; Adam, M.; Silva, M. D.; Sheiko, S. S.; Rubinstein, M. *Macromolecules* **2004**, *37*, 5002−5005.
(38) Hentze, H. P.; Kramer, E.; Berton, B.; Forster, S.; Antonietti, M. *Macromolecules* **1999**, *32*, 5803−5809.
(39) Fu, J.; Luan, B.; Yu, X.; Cong, Y.; Li, J.; Pan, C.; Han, Y.; Yang, Y.; Li, B. *Macromolecules* **2004**, *37*, 976−986.
(40) Zhang, W.; Shi, L.; An, Y.; Gao, L.; Wu, K.; Ma, R. *Macromolecules* **2004**, *37*, 2551−2555.
(41) Soo, P. L.; Eisenberg, A. *J. Polym. Sci., Part B* **2004**, *42*, 923−938.
(42) Liang, X.; Mao, G.; Ng, K. *Colloids Surf. B* **2004**, *34*, 41−51.
(43) Forster, S.; Berton, B.; Hentze, H. P.; Kramer, E.; Antonietti, M. *Macromolecules* **2001**, *34*, 4610−4623.
(44) Hentze, H. P.; Kaler, E. W. *Curr. Opin. Colloid Interface Sci.* **2003**, *8*, 164−178.
(45) Won, Y.; Davis, H. T.; Bates, F. S. *Science* **1999**, *283*, 960−962.
(46) Velegol, S. B.; Logan, B. E. *Langmuir* **2002**, *18*, 5256−5262.
(47) Colton, R. J.; Baselt, D. R.; Dufrene, Y. F.; Green, J. D.; Lee, G. U. *Curr. Opin. Chem. Biol.* **1997**, *1*, 370−377.
(48) Ducker, W. A.; Senden, T. J. *Langmuir* **1992**, *8*, 1831−1836.
(49) Muller, D.; Engel, A. *Biophys. J.* **1997**, *73*, 1633−1644.
(50) Heinz, W. F.; Hoh, J. H. *Nanotechnology* **1999**, *17*, 143−150.
(51) Klushin, L. I.; Skvortsov, A. M.; Leermakers, F. A. M. *Phys. Rev. A* **2004**, *69*, 061101.
(52) Leermakers, F. A. M.; Gorbunov, A. A. *Macromolecules* **2002**, *35*, 8640−8649.

(53) O'Shea, S. J.; Welland, M. E.; Rayment, T. *Langmuir* **1993**, *9*, 1826−1835.
(54) Butt, H.-J.; Kappl, M.; Mueller, H.; Raiteri, R. *Langmuir* **1999**, *15*, 2559−2565.
(55) Currie, E. P. K.; Gucht, J. V.; Borisov, O. V.; Cohen-Stuart, M. A. *Pure Appl. Chem.* **1999**, *71*, 1227−1241.
(56) Srinivas, G.; Discher, D. E.; Klein, M. L. *Nat. Mater.* **2004**, *3*, 638−644.
(57) Webber, G. B.; Wanless, E. J.; Butun, V.; Armes, S. P.; Biggs, S. *Nano Lett.* **2002**, *2*, 1307−1313.
(58) Nalaskowski, J.; Veeramasuneni, S.; Hupka, J.; Miller, J. D. *J. Adhes. Sci. Technol.* **1999**, *13*, 1519−1533.
(59) Dalhaimer, P.; Bates, F. S.; Discher, D. E. *Macromolecules* **2003**, *36*, 6873−6877.

MA047858J